

Cite this: *Chem. Sci.*, 2012, **3**, 2993

www.rsc.org/chemicalscience

EDGE ARTICLE

# Selective CO<sub>2</sub> uptake and inverse CO<sub>2</sub>/C<sub>2</sub>H<sub>2</sub> selectivity in a dynamic bifunctional metal–organic framework†

Wenbin Yang,<sup>a</sup> Andrew J. Davies,<sup>a</sup> Xiang Lin,<sup>a</sup> Mikhail Suyetin,<sup>a</sup> Ryotaro Matsuda,<sup>bc</sup> Alexander J. Blake,<sup>a</sup> Claire Wilson,<sup>a</sup> William Lewis,<sup>a</sup> Julia E. Parker,<sup>d</sup> Chiu C. Tang,<sup>d</sup> Michael W. George,<sup>a</sup> Peter Hubberstey,<sup>a</sup> Susumu Kitagawa,<sup>bc</sup> Hirotohi Sakamoto,<sup>bc</sup> Elena Bichoutskaia,<sup>a</sup> Neil R. Champness,<sup>a</sup> Sihai Yang<sup>\*a</sup> and Martin Schröder<sup>\*a</sup>

Received 13th April 2012, Accepted 13th June 2012

DOI: 10.1039/c2sc20443f

The unique bifunctional porous metal–organic framework, [Co(HL<sup>dc</sup>)]·1.5MeOH·dioxane, incorporates both free-standing carboxyl and pyridyl groups within its pores. Gas adsorption measurements on the desolvated framework reveal unusual selective CO<sub>2</sub> adsorption over C<sub>2</sub>H<sub>2</sub> and CH<sub>4</sub> linked to a framework phase change from a narrow pore (*np*) to a large pore (*lp*) form, mediated by CO<sub>2</sub> uptake at 195 K. This phase transition has been monitored by *in situ* powder X-ray diffraction and IR spectroscopy, and modelled by Grand Canonical Monte Carlo simulations revealing that the reversible *np* to *lp* transition is linked to the rotation of pyridyl rings acting as flexible “pore gates”.

## Introduction

Metal–organic frameworks (MOFs) are attracting considerable attention as promising hybrid materials with applications in gas storage<sup>1,2</sup> and separation,<sup>3</sup> heterogeneous catalysis,<sup>4</sup> and drug delivery.<sup>5</sup> These porous materials form well-ordered extended structures and have enormous design flexibility.<sup>6–8</sup> Since the pore walls of MOFs typically comprise organic bridging ligands, the incorporation of additional functional groups<sup>9</sup> into the linking ligand tecton potentially affords frameworks in which these extra groups protrude into the pores or are part of the channel wall.<sup>4,9–15</sup> However, since polar donor organic groups tend necessarily to engage in framework building *via* binding to metal centres or hydrogen bonding, it remains a challenge to obtain porous MOFs directly in which the pore surfaces are decorated with well-defined free-standing functional polar organic sites.

We sought to design and synthesise polydonor ligands incorporating *exo*-binding carboxylate and amine donors coupled to other donor groups that are sterically compromised. This methodology will necessarily leave specific ligand donor groups free-standing and available within the resultant porous solid. We report herein the synthesis, structural characterisation and gas sorption properties of two novel bifunctional acid/base-containing complexes [Co(HL<sup>dc</sup>)]·1.5MeOH·dioxane (**1**) and [Co(HL<sup>dc</sup>)]·2DMF·H<sub>2</sub>O (**2**), which represent unusual examples of porous MOFs in which the channels are simultaneously functionalised by both free acidic carboxylic and free basic pyridyl groups. Upon desolvation of **1** the resulting porous solid, **1a**, exhibits selectivity for CO<sub>2</sub> adsorption over C<sub>2</sub>H<sub>2</sub> and CH<sub>4</sub>, and this has been studied using *in situ* structural and spectroscopic techniques and modelled using Grand Canonical Monte Carlo simulations.

## Results and discussion

Solvothermal reaction of H<sub>4</sub>L (Scheme 1) incorporating seven potential donor sites (two types of pyridyl and two types of

<sup>a</sup>School of Chemistry, University of Nottingham, University Park, Nottingham, UK NG7 2RD. E-mail: Sihai.Yang@nottingham.ac.uk; Tel: +44 (0)115 9513452; m.schröder@nottingham.ac.uk; +44 (0)115 9513490

<sup>b</sup>ERATO Kitagawa Integrated Pores Project, Science and Technology Agency (JST), Kyoto Research Park Bldg#3, Shimogyo-ku, Kyoto, 600-8815, Japan

<sup>c</sup>Institute for Integrated Cell-Material Science (iCeMS), Kyoto University, Yoshida, Sakyo-ku, Kyoto, 606-8501, Japan

<sup>d</sup>Diamond Light Source, Harwell Science and Innovation Campus, Didcot, Oxfordshire, UK OX11 0DE

† Electronic supplementary information (ESI) available: Details of analyses of crystal structures, CIF files for complexes **1** and **2**, PXRD and TGA data, and technical details for gas adsorption experiments, gas isotherms and their analysis. CCDC reference numbers 743187 and 743188. For ESI and crystallographic data see DOI: 10.1039/c2sc20443f



**Scheme 1** *In situ* decarboxylation of H<sub>4</sub>L to give [HL<sup>dc</sup>]<sup>2-</sup> in **1** and **2**, and view of binding of [HL<sup>dc</sup>]<sup>2-</sup> to Co(II) showing non-coordinated pendant acidic and basic sites (Co: turquoise; O: red; N: blue; C: grey; H: white).

carboxylate groups) with  $\text{Co}(\text{NO}_3)_2 \cdot 6\text{H}_2\text{O}$  in  $\text{MeOH}/1,4$ -dioxane (v/v 4 : 1) at 130 °C for 3 days led to *in situ* decarboxylation of  $\text{H}_4\text{L}$  (Scheme 1) and formation of  $[\text{Co}(\text{HL}^{\text{dc}})] \cdot 1.5\text{MeOH} \cdot \text{dioxane}$ , **1**, as purple columnar crystals. At lower temperature (90 °C) the solvothermal reaction of  $\text{H}_4\text{L}$  with  $\text{Co}(\text{NO}_3)_2 \cdot 6\text{H}_2\text{O}$  in  $\text{DMF}/\text{H}_2\text{O}$  (v/v 5 : 1) afforded purple tabular crystals of a similar decarboxylated product  $\{[\text{Co}(\text{HL}^{\text{dc}})] \cdot 2\text{DMF} \cdot \text{H}_2\text{O}\}_\infty$ , **2**, incorporating different guest solvent molecules. No decarboxylation of  $\text{H}_4\text{L}$  occurs under the same solvothermal conditions in the absence of  $\text{Co}(\text{II})$  salt, suggesting that  $\text{Co}(\text{II})$  plays a crucial role in the decarboxylation process. *In situ* decarboxylation under hydro(solvo)thermal conditions has been reported previously in which the metal ions play a unique catalytic role in the decarboxylation process,<sup>16,17</sup> although decarboxylation reactions are also known to occur in the absence of transition metal ions.<sup>18</sup>

**1** crystallises in the monoclinic space group  $P2_1/c$ . Each  $\text{Co}(\text{II})$  ion in **1** is five coordinate and bound to three carboxylate oxygen atoms and two pyridyl N-donors from four distinct  $[\text{HL}^{\text{dc}}]^{2-}$  ligands resulting in a distorted trigonal bipyramidal coordination sphere. In turn, each  $[\text{HL}^{\text{dc}}]^{2-}$  ligand links to four different  $\text{Co}(\text{II})$  centers *via* two carboxylate groups of the isophthalate moiety and two external pyridyl arms of the terpy unit. The interconnection of  $\text{Co}(\text{II})$  centres and  $[\text{HL}^{\text{dc}}]^{2-}$  affords an extended 3D porous framework (Fig. 1a) exhibiting the (3,4)-connected  $(8^3)_2(8^6)$  **tfa**<sup>19</sup> topology (Fig. S2†). The most remarkable feature is that in each  $[\text{HL}^{\text{dc}}]^{2-}$  ligand neither the internal pyridyl amine of the terpy unit nor the carboxylic group on this internal pyridyl ring coordinate to the metal nodes, nor do they form any hydrogen bonds with atoms at the pore surface. Therefore, these groups are free-standing and potentially available for intermolecular interactions within the pore channels of **1**. Although functionalised MOFs containing free  $-\text{COOH}$ ,  $-\text{OH}$ ,  $-\text{NH}_2$  or pyridyl groups have been reported,<sup>4,9–14</sup> **1** represents a distinct example of a porous host incorporating two different types of free organic binding sites within its channels. The dangling carboxylic groups and electron-donating N-centres on the pore surface of **1a** endow the framework with a new level of flexibility and complexity, exceeding that of any simple framework with a homogenous pore environment.

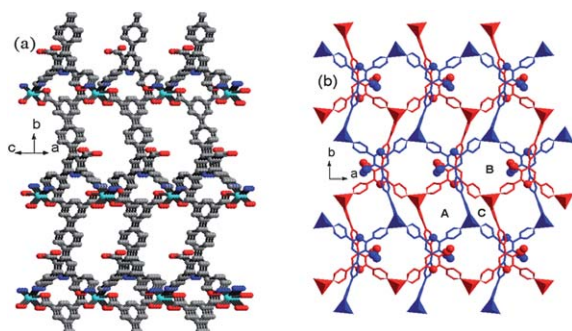


**Fig. 1** Single crystal X-ray structure of **1**. (a) View of the 3D nanoporous single network for **1** (H atoms are omitted for clarity). (b) View of three types of distinct channels formed along the *c* axis following double network interpenetration shown in blue and red, respectively. Uncoordinated carboxyl and pyridyl groups are highlighted as space-filling nodes.

Another interesting structural feature of **1** is that upon two-fold interpenetration three distinct channels are formed along the *c* axis (Fig. 1b). Channel **A** (diameter: *ca.* 6.3 Å) is surrounded by the aromatic faces of phenyl groups and coordinated pyridyl rings of  $[\text{HL}^{\text{dc}}]^{2-}$  ligands, with both the uncoordinated internal pyridyl amines and  $\text{Co}(\text{II})$  polyhedra located at the corners of the channel. Channel **A** is filled with methanol molecules. Uncoordinated carboxyl groups protrude into channel **B** (diameter: *ca.* 5.9 Å), and these channels are filled with both  $\text{MeOH}$  and 1,4-dioxane molecules. Channel **C** (diameter: *ca.* 1.1 Å) is too small to accommodate any solvent molecules. The solvent void for **1** was estimated using PLATON/SOLV<sup>20</sup> to be 38.0% of the unit cell volume. Although compound **2** crystallises in the triclinic space group  $P\bar{1}$ , it has very similar structural features and the same topology as **1** (see ESI†).

**1** undergoes successive weight losses by thermal gravimetric analysis from room temperature to 250 °C (Fig. S4†) corresponding to the release of free  $\text{MeOH}$  and dioxane molecules (calcd 19.2%; found 18.2%). The fully desolvated framework, **1a**, obtained by heating the as-synthesised sample of **1** at 125 °C under vacuum ( $10^{-8}$  mbar) for 12 h remains crystalline with the observed PXRD pattern matching well the calculated pattern derived from the single crystal structure of **1** (Fig. S5†).

Adsorption isotherms of several light gases ( $\text{N}_2$ ,  $\text{CO}_2$ ,  $\text{H}_2$ ,  $\text{CH}_4$  and  $\text{C}_2\text{H}_2$ ) were recorded on the desolvated polycrystalline sample of **1a**. The  $\text{N}_2$  isotherm at 77 K shows a two-step process with a small but noticeable second step observed at 0.26 bar; the desorption branch retraces the adsorption isotherm (Fig. 2a). The Langmuir and BET surface areas for the first adsorption process, calculated from the  $\text{N}_2$  adsorption isotherm data, are 936 and 773  $\text{m}^2 \text{g}^{-1}$ , respectively. The total pore volume estimated from DR plots is 0.328  $\text{cm}^3 \text{g}^{-1}$ , close to the calculated crystallographic pore volume of 0.352  $\text{cm}^3 \text{g}^{-1}$  of **1a**. The average pore size determined by applying the DA equation for the  $\text{N}_2$  sorption data is 6.2 Å with a narrow distribution (Fig. S6†), consistent with the values estimated from the single crystal X-ray structure determination of **1** (Fig. 1b). At 77 K, **1a** adsorbs  $\text{H}_2$  gas up to *ca.* 1.18 wt% at 0.2 bar, increasing to 1.62 wt% at 1.0 bar, and finally attaining a near saturated level of 2.28 wt% at 20 bar (Fig. S10†). The maximum uptake of  $\text{H}_2$  in **1a** is relatively low in comparison to the highest capacity materials,<sup>21–23</sup> but consistent with the limited pore volume and surface areas and narrow pore channels observed in **1a**.

At 195 K,  $\text{CO}_2$  sorption proceeds in two pronounced consecutive steps (Fig. 2a): after a very fast uptake ( $143.5 \text{ cm}^3 \text{g}^{-1}$ ) at low pressure, the isotherm reaches a plateau between 0.03 bar and 0.10 bar, followed by another significant increase in gas uptake, and finally at 1.0 bar an uptake of 239.5  $\text{cm}^3 \text{g}^{-1}$  is measured. The desorption isotherm does not trace the adsorption branch, and therefore gives a hysteresis loop. The maximum  $\text{CO}_2$  uptake of **1a** is lower than some of the best behaving MOFs<sup>21,22,23f</sup> due to the limited available pore volume. At 195 K, the two-step isotherm loop observed for  $\text{CO}_2$  sorption involves two forms of **1a**: a narrow pore (*np*) form at  $\text{CO}_2$  pressures below 100 mbar and a large pore (*lp*) form at  $\text{CO}_2$  pressure above 100 mbar.<sup>24–29</sup> This phase transition is not immediately reversible, because the transition pressure at adsorption (125 mbar) is higher than that at desorption (83 mbar). Thus, a hysteresis loop is observed (Fig. 2a). The total pore volume of the *np* form is estimated to be

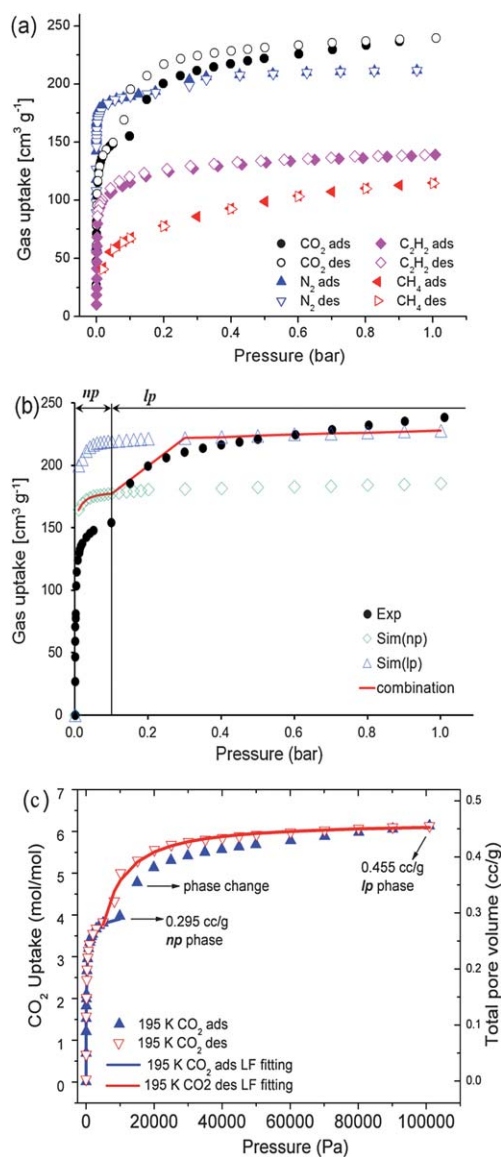


**Fig. 2** Gas sorption profiles for **1a**. (a) Isotherms for CO<sub>2</sub> (black), C<sub>2</sub>H<sub>2</sub> (purple) and CH<sub>4</sub> (red) at 195 K, and N<sub>2</sub> isotherm (blue) at 77 K. (b) Comparison of 195 K CO<sub>2</sub> isotherms for experiment (black filled circles), *np* simulation (green diamonds), *lp* simulation (blue triangles) and combined simulations (red line) at 195 K. (c) Langmuir–Freundlich (LF) fittings of the CO<sub>2</sub> sorption isotherm and analysis of pore volume changes on CO<sub>2</sub> sorption at 195 K (filled symbols: adsorption; open symbols: desorption).

0.295 cm<sup>3</sup> g<sup>-1</sup> from DR analysis applied to the CO<sub>2</sub> data in the low pressure region (first plateau) using a density of 1.032 g cm<sup>-3</sup> for liquid CO<sub>2</sub>. This is consistent with the values calculated from the N<sub>2</sub> isotherm (0.328 cm<sup>3</sup> g<sup>-1</sup>) and from the crystal structure (0.352 cm<sup>3</sup> g<sup>-1</sup>) of **1a**, indicating that the *np* form is very similar to that of the original desolvated structure. At higher CO<sub>2</sub> pressures, the structure pores expand to the *lp* phase which has a total pore volume of 0.455 cm<sup>3</sup> g<sup>-1</sup>, leading to a ~50% increase on the total pore volume and consistent with the GCMC simulation results (see below). The Langmuir surface area of the *lp* form, measured from the CO<sub>2</sub> isotherm at 195 K, is 1143 m<sup>2</sup> g<sup>-1</sup>, higher than that determined (936 m<sup>2</sup> g<sup>-1</sup>) for the *np* form from N<sub>2</sub> uptake

data at 77 K. The enhanced Langmuir surface area also confirms the expansion of the porous structure **1a** from the *np* to *lp* form, which then allows additional uptake of CO<sub>2</sub>.

To probe the nature of this transition, we carried out Grand Canonical Monte Carlo (GCMC) modelling of the CO<sub>2</sub> adsorption isotherms for **1a**. We found that **1a** has flexible “gates” in the form of the pyridyl rings, which through their rotation provide additional pore volume for CO<sub>2</sub> adsorption. Thus, entry of guest molecules into the pores in the *np* and *lp* phases can be controlled *via* a structural dynamic effect of “gate” opening as illustrated in Fig. 3 in which the initial narrow pore *np* phase affords the large pore *lp* phase *via* rotation of left and right rings (Fig. 3, top) by 40 and 60°, respectively, leading to an almost 50% increase in the total pore volume. The GCMC simulations have been performed for both *np* and *lp* pores, and theoretical gas sorption profiles for both *np* and *lp* phases are shown in Fig. 2b. The adsorption behavior of CO<sub>2</sub> between 0 bar and 0.1 bar is thus explained by the filling of the *np* pore, whereas at 0.1 bar the pyridyl rings rotate under pressure leading to an increase in the observed pore volume. Subsequently, a gradual, rather than an abrupt, change in the CO<sub>2</sub> uptake from 0.1 bar to 0.3 bar is observed. The combination of the theoretical *np* and *lp* isotherms gives an excellent agreement with the observed experimental data.

The symmetric CO<sub>2</sub> molecule has a permanent quadrupole moment which interacts with the MOF lattice, and this effect leads to the “gate” opening mechanism thus allowing additional gas to enter. The same phenomenon does not occur for the CH<sub>4</sub> adsorption process under the same conditions (Fig. 2a) due to the absence of a quadrupole moment and thus the pores remain more rigid. Interestingly, although it has a permanent quadrupole moment, C<sub>2</sub>H<sub>2</sub> adsorption at 195 K does not lead to the

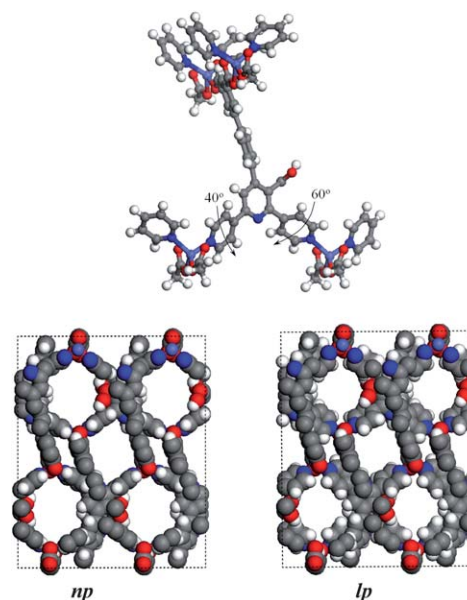


**Fig. 3** (Top) The transition between a narrow pore (*np*) form and a large pore (*lp*) form *via* rotation of the left and right pyridyl rings by 40 and 60°, respectively. (Bottom) Effect of the rotation of the pyridyl rings on the size of the pore: a narrow pore (*np*) form and a large pore (*lp*) form of the framework.

presence of similar “gate” rotation. This is probably due to the adsorption temperature being higher than the boiling point (189 K) of  $C_2H_2$ , and thus additional  $C_2H_2$  uptake is required to trigger this “gate” rotation. This mechanism is fully supported by further analysis of the  $CO_2$  isotherms, by consideration of  $CO_2$  adsorption thermodynamics, and, significantly, by *in situ* PXRD studies of **1a** as a function of  $CO_2$  loading (see below). At 273 K, however, the  $CO_2$  isotherm shows a typical Type-I isotherm without steps or hysteresis (Fig. S7†); the  $CO_2$  storage capacity is  $108\text{ cm}^3\text{ g}^{-1}$  at 1.0 bar, increasing to  $145\text{ cm}^3\text{ g}^{-1}$  at 10 bar. Thus, no phase transition is observed at 273 K, confirming that the framework flexibility in **1a** is not only  $CO_2$ -induced but is also temperature dependent.

To calculate the free-energy difference ( $\Delta F_{\text{host}}$ ) between the two guest-free forms, we applied a modified equation (see ESI†) which can be derived from the thermodynamic model recently developed to analyse the  $CO_2$  isotherms for MIL-53<sup>27,28</sup> and DMOF-1-AM<sup>29</sup> materials. The  $CO_2$  sorption isotherms can be fitted to this model very well, as shown in Fig. 2c and Table S6.† The  $\Delta F_{\text{host}}$  estimated from the fitting results was found to be between 8–17 kJ mol<sup>-1</sup>. This value is relatively small compared with MIL-53 and DMOF-1-AM2, but is comparable to that observed for DMOF-1-AM3, indicating a relatively small difference in energy between the *np* and *lp* phases of **1a**.

*In situ* powder X-ray diffraction studies at various  $CO_2$  pressures (0–1 bar) were carried out at 195 K to track the framework transition during the adsorption/desorption process. The diffraction patterns of solvated **1** and of desolvated **1a** at 195 K under 0, 71, 222, 622, and 1000 mbar of  $CO_2$  adsorption loadings and at 210 and 0 mbar of  $CO_2$  desorption loadings were recorded (Fig. 4). Powder X-ray diffraction of **1a** (0 mbar) confirms that the framework remains intact on desolvation and degassing, and no apparent peak changes were observed up to 70 mbar  $CO_2$  loadings, confirming retention of the original *np* phase at low  $CO_2$  pressures. At  $CO_2$  pressures of 222 mbar and above, shifts in the peaks (110), (1 $\bar{1}$ 1), (1 $\bar{1}$ 2) and splitting of peaks (011), (021), (040), (210), (220), (150), (2 $\bar{3}$ 1), (002) were observed in the

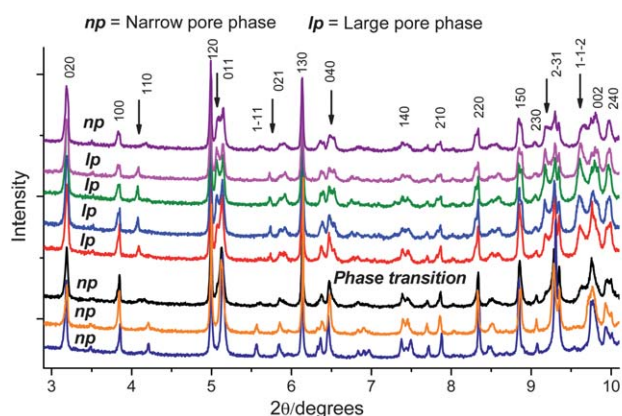


**Fig. 4** *In situ* synchrotron powder X-ray diffraction patterns with peak indices at different  $CO_2$  adsorption/desorption loadings at 195 K for **1a** (data collected at Diamond Light Source,  $\lambda = 0.82559\text{ \AA}$ ). (a) Original sample **1**. (b) Degassed sample **1a**. (c) 70.7 mbar adsorption; (d) 222 mbar adsorption; (e) 602 mbar adsorption; (f) 1000 mbar adsorption; (g) 210 mbar desorption. (h) Final degassed sample at 0 mbar  $CO_2$ . The apparent changes of peaks are marked with arrows.

diffraction patterns, confirming a structural change and the formation of the *lp* phase at high pressures. On removal of  $CO_2$ , the final degassed material shows peaks entirely consistent with the re-formation of the original *np* phase, confirming the reversibility of this transition process. Although shifts and changes of peaks are observed at high  $CO_2$  loadings, the unit cell parameters do not change very much, suggesting the nature of the *np* and *lp* phases are structurally similar. These results strongly support and are entirely consistent with the “gate-rotation” transition mechanism proposed from the GCMC modelling study.

To investigate further this interesting  $CO_2$ /host system, we probed the  $CO_2$  sorption process in **1a** by *in situ* IR spectroscopy by monitoring the combination vibrations of  $CO_2$  in the region  $3500\text{--}3800\text{ cm}^{-1}$ . The two combination bands, centred at  $3714$  and  $3612\text{ cm}^{-1}$ , have a lower intensity than the fundamental antisymmetric stretch at  $2348\text{ cm}^{-1}$ . This latter band has an absorbance of much greater than 1.0 at pressures above 0.2 bar in our apparatus, and is therefore too intense to be recorded precisely and used as a probe. A low spectral resolution ( $2\text{ cm}^{-1}$ ) was used to allow for efficient subtraction of the background gaseous  $CO_2$ . Measurements of  $CO_2$  in a KBr disc in the absence of **1a** show the two IR combination bands, which increase in intensity with increasing  $CO_2$  pressure (Fig. 5a). As the sample of **1a** was exposed to increasing pressures of  $CO_2$  gas, from 0–1 bar, two new IR bands were clearly observed to grow in at  $3690$  and  $3582\text{ cm}^{-1}$  (Fig. 5b). The new bands were also observed in the fundamental  $CO_2$  region of the spectrum at  $2334$  and  $2270\text{ cm}^{-1}$  (data not shown). By comparison to the bands of free  $CO_2$ , the new bands observed (Fig. 5c) were consistent with the formation of a single adsorbed  $CO_2$  species in **1a**. We have examined the concentration of the adsorbed  $CO_2$  by integrating the areas under the peaks at  $3690$  and  $3582\text{ cm}^{-1}$ , and Fig. 6 shows the

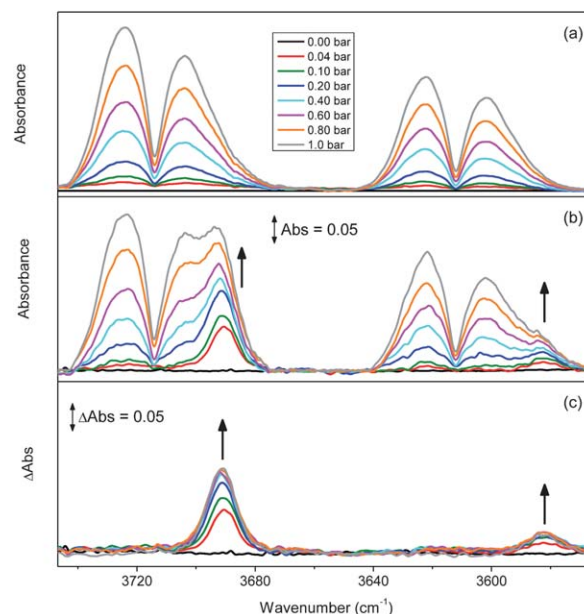


**Fig. 5** *In situ* FTIR spectra of gaseous  $CO_2$  at various pressures (0–1 bar) in the combination region at 195 K: (a) KBr, (b) KBr + **1a**, and (c) the difference spectra, showing the growth of two new bands. Arrows indicate the growth of bands due to adsorbed  $CO_2$  with increasing pressure.

changes in these band areas with increasing pressure. The results have been normalised such that the final absorption of the 3690 and 3582  $\text{cm}^{-1}$  are set to 1.0 at 1 bar. There is a rapid increase in the absorption bands at 3690 and 3582  $\text{cm}^{-1}$  at low pressures, and the change in IR absorption reaches a plateau between 0.03 and 0.1 bar, followed by another significant increase in gas uptake above 0.1 bar. Thus, the increase in the areas under the IR bands on  $\text{CO}_2$  inclusion is entirely consistent with the data from the gas sorption isotherm, both showing two pronounced consecutive steps occurring at the same pressure regions (Fig. 3c, Fig. 6), thus confirming the distinct two-step  $\text{CO}_2$  uptake by **1a**.

The behavior of **1a** on  $\text{CO}_2$  sorption becomes more significant when it is compared to that of  $\text{CH}_4$  and particularly  $\text{C}_2\text{H}_2$ . In the case of  $\text{CH}_4$  a reversible Type-I isotherm was observed showing that **1a** can store up to 115  $\text{cm}^3 \text{g}^{-1}$  of  $\text{CH}_4$  at 195 K and 1.0 bar, less than half of the  $\text{CO}_2$  uptake (240  $\text{cm}^3 \text{g}^{-1}$ ) under the same conditions (Fig. 2a). Such a difference between  $\text{CO}_2$  and  $\text{CH}_4$  adsorption capacities of **1a** could be exploited in natural gas separation processes.

**1a** shows good acetylene uptake, with high reversibility between adsorption and desorption isotherms at 195 K (Fig. 2a). The  $\text{C}_2\text{H}_2$  uptake at 1.0 bar is 140  $\text{cm}^3 \text{g}^{-1}$ , higher than for organic molecular porous materials such as cucurbit[6]uril,<sup>30</sup> and for most previously studied porous MOFs,<sup>31–33</sup> with the notable exceptions of  $[\text{M}_2(\text{L})_2(\text{dabco})]$  ( $\text{M} = \text{Zn}, \text{Cu}$ ;  $\text{L}^{2-} = 1,4\text{-benzenedicarboxylate}, \text{naphthalene-2,6-dicarboxylate}$ ; dabco = 1,4-diazabicyclo[2.2.2]octane).<sup>34</sup> The  $\text{C}_2\text{H}_2/\text{CO}_2$  uptake ratio can be used to estimate the relative affinity of  $\text{CO}_2$  and  $\text{C}_2\text{H}_2$  towards the functional pore surface. Significantly, at 195 K **1a** shows high selectivity for  $\text{CO}_2$  over  $\text{C}_2\text{H}_2$ , with  $\text{C}_2\text{H}_2/\text{CO}_2$  uptake ratios of 0.72 : 1 at 0.01 bar (94  $\text{cm}^3 \text{g}^{-1} \text{C}_2\text{H}_2/131 \text{cm}^3 \text{g}^{-1} \text{CO}_2$ ); 0.74 : 1 at 0.1 bar (115  $\text{cm}^3 \text{g}^{-1} \text{C}_2\text{H}_2/155 \text{cm}^3 \text{g}^{-1} \text{CO}_2$ ); 0.58 : 1 at 1.0 bar (140  $\text{cm}^3 \text{g}^{-1} \text{C}_2\text{H}_2/240 \text{cm}^3 \text{g}^{-1} \text{CO}_2$ ). Such inverse selectivity for  $\text{CO}_2$  over  $\text{C}_2\text{H}_2$  is particularly noteworthy as this selectivity is opposite to the high  $\text{C}_2\text{H}_2/\text{CO}_2$  uptake ratios observed for MOFs such as 1.35 : 1 for  $\text{Mn}(\text{HCOO})_2$  and 1.47 : 1 for  $\text{Mg}(\text{HCOO})_2$ .<sup>31</sup> Adsorption of  $\text{C}_2\text{H}_2$  is typically favoured in MOFs due to enhanced substrate/adsorbate interactions for  $\text{C}_2\text{H}_2$  over  $\text{CO}_2$ .<sup>35</sup>

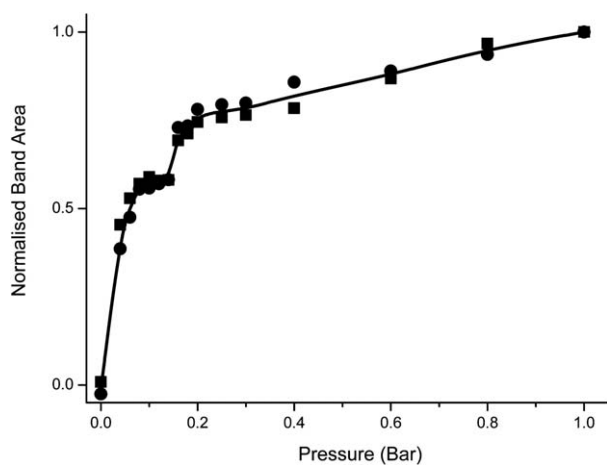


**Fig. 6** Plot showing the normalised band areas of the peaks at 3690 (●) and 3582  $\text{cm}^{-1}$  (■) as a function of  $\text{CO}_2$  pressure. The areas were averaged at each pressure to produce a point-to-point average (black line).

Thus, the observed selectivity of  $\text{CO}_2$  over  $\text{C}_2\text{H}_2$  is highly unusual and is attributed to the  $\text{CO}_2$  gas-specific framework transition from the *np* to *lp* phase at 195 K, mediated by the rotation of pyridyl rings on the ligand.

## Conclusions

We have prepared and characterised a novel porous bifunctional hybrid material **1** incorporating both pendant carboxyl and pyridyl groups in the channels. The corresponding desolvated form **1a** shows reasonable uptake capacities for  $\text{H}_2$ ,  $\text{C}_2\text{H}_2$  and  $\text{CH}_4$ . Noticeably and significantly,  $\text{CO}_2$ -framework interactions result in a reversible structural transition for **1a** between *np* and *lp* forms, allowing additional  $\text{CO}_2$  uptake leading to a high total adsorption of  $\text{CO}_2$ . At 195 K, the  $\text{CO}_2$  sorption isotherm of **1a** exhibits two pronounced steps arising from the rotation of pyridyl rings. Our GCMC simulations confirm that the pyridyl rings act as flexible “gates”, which at 0.1 bar rotate under the pressure leading to an overall increase in pore volume. This is also consistent with the observations from *in situ* PXRD and IR experiments. In contrast,  $\text{C}_2\text{H}_2$  and  $\text{CH}_4$  do not induce such structural transformations under the same conditions, and this results in lower uptakes. These results indicate that **1a** and its analogues have the potential to emerge as important functional materials for fuel gas purification with particular interest in the  $\text{CO}_2/\text{C}_2\text{H}_2$  separation process.

## Materials and methods

### Synthesis of ligand $\text{H}_4\text{L}$

$\beta$ -Amino- $\beta$ -(pyrid-4-yl)acrylonitrile (0.58 g, 4 mmol) and 4-bromobenzaldehyde (0.37 g, 2 mmol) were mixed in  $\text{CH}_3\text{COOH}$  (15 ml) and heated at 120  $^\circ\text{C}$  for 2 days. The resultant mixture was evaporated to almost dryness, and then triturated with water. The solid product was collected by filtration and recrystallised from ethanol/ $\text{H}_2\text{O}$  (10 : 1 v/v) to afford 3',5'-dicyano-4-(*p*-bromophenyl)-4,2':6',4''-terpyridine as a pale yellow crystalline solid. Elemental analysis for  $\text{C}_{23}\text{H}_{12}\text{BrN}_5$  (calcd/found): C, 63.03/63.06; H, 2.76/2.75; N, 15.98/16.01; IR (KBr,  $\nu_{\text{max}}$ ): 2205  $\text{cm}^{-1}$ ;  $^1\text{H-NMR}$  ( $\text{DMSO-}d_6$ ): 8.86 (m, 4H), 8.05 (d, 4H), 7.78 (d, 2H) and 7.59 (d, 2H).

A mixture of 3',5'-dicyano-4-(*p*-bromophenyl)-4,2':6',4''-terpyridine (0.44 g, 1 mmol),  $\text{K}_2\text{CO}_3$  (1.38 g, 10 mmol) and diethyl isophthalate-5-boronic acid (0.27 g, 1 mmol) in DMF (30 ml) and  $\text{H}_2\text{O}$  (10 ml) was de-aerated with  $\text{N}_2$  for 20 min. To this mixture was added  $\text{Pd}(\text{PPh}_3)_4$  (28 mg, 0.024 mmol) and the reaction mixture heated at 90  $^\circ\text{C}$  for 5 days under  $\text{N}_2$ . The resultant mixture was evaporated to dryness under reduced pressure, extracted into  $\text{CHCl}_3$  and dried over  $\text{MgSO}_4$ . Removal of  $\text{CHCl}_3$  gave a pale white solid, which was treated with KOH (2 M, 100 ml) and refluxed for 2 days to afford a slightly yellow solution. The solution was acidified with conc. HCl (37%) to yield  $\text{H}_4\text{L}$  (0.44 g, 78%) as an off-white solid. Elemental analysis for  $\text{C}_{31}\text{H}_{19}\text{N}_3\text{O}_8$  (calcd/found): C, 66.31/66.28; H, 3.41/3.39; N, 7.48/7.50; IR (KBr,  $\nu_{\text{max}}$ ): 3423, 3084, 1702, 1674, 1633, 1597, 1541, 1505, 1384, 1249, 1103, 834, 793, 761, 671  $\text{cm}^{-1}$ ;  $^1\text{H-NMR}$  ( $\text{DMSO-}d_6$ ): 8.80 (d, 4H), 8.50 (s, 1H), 8.45 (s, 2H), 8.33 (d, 4H), 7.90 (d, 2H), 7.82 (d, 2H).

## Synthesis of $\{[\text{Co}(\text{HL}^{\text{dc}})] \cdot 1.5\text{MeOH} \cdot \text{dioxane}\}_{\infty}$ (**1**) and $\{[\text{Co}(\text{HL}^{\text{dc}})] \cdot 2\text{DMF} \cdot \text{H}_2\text{O}\}_{\infty}$ (**2**)

Similar experimental procedures were employed in the syntheses of **1** and **2**. H<sub>4</sub>L (28.1 mg, 0.05 mmol) and Co(NO<sub>3</sub>)<sub>2</sub>·6H<sub>2</sub>O (19.8 mg, 0.07 mmol) were mixed in MeOH/1,4-dioxane (4 : 1 v/v, 10 ml), sealed in a 23 cm<sup>3</sup> Parr bomb and heated to 130 °C at the rate of 0.5 °C per minute. After 3 days the temperature was reduced to room temperature at the rate of 0.1 °C min<sup>-1</sup>. Purple columnar crystals of **1** were isolated, washed with methanol and dried in air (25.2 mg; 52.3% yield). Elemental analysis for **1** [Co(C<sub>30</sub>H<sub>17</sub>O<sub>6</sub>N<sub>3</sub>)(CH<sub>3</sub>OH)<sub>1.5</sub>(C<sub>4</sub>H<sub>8</sub>O<sub>2</sub>) (calcd/found): C, 60.01/59.98; H, 4.40/4.42; N, 5.91/5.93; selected IR (KBr, ν<sub>max</sub>): 3363, 2856, 1666, 1617, 1576, 1438, 1367, 1289, 1254, 1220, 1117, 1080, 889, 870, 841, 778, 732, 691, 597 cm<sup>-1</sup>. The solvothermal reaction of H<sub>4</sub>L (29.1 mg, 0.052 mmol) with Co(NO<sub>3</sub>)<sub>2</sub>·6H<sub>2</sub>O (18.0 mg, 0.062 mmol) in DMF/H<sub>2</sub>O (v/v = 5 : 1, 6 ml) at 90 °C for 2 days afforded purple tablet crystals of **2**, and the crystals were collected by filtration, washed with MeOH and dried in air (16.4 mg, 35.8%). Elemental analysis for **2** [Co(C<sub>30</sub>H<sub>17</sub>O<sub>6</sub>N<sub>3</sub>)(C<sub>3</sub>H<sub>7</sub>NO<sub>2</sub>)(H<sub>2</sub>O) (calcd/found): C, 58.54/58.57; H, 4.50/4.48; N, 9.48/9.52; selected IR (KBr, ν<sub>max</sub>): 3382, 2929, 1660, 1616, 1579, 1501, 1437, 1383, 1297, 1253, 1221, 1096, 1069, 915, 870, 841, 803, 777, 728, 689 cm<sup>-1</sup>.

### X-Ray crystallographic studies of **1** and **2**

X-Ray diffraction data from single crystals of **1** and **2** were collected at 150(2) K on a Bruker SMART APEX or a Bruker SMART1000 CCD area detector diffractometer using graphite-monochromated Mo-Kα radiation (λ = 0.71073 Å), equipped with an Oxford Cryosystems open-flow cryostat. An empirical absorption correction was applied to the intensity data using SADABS.<sup>36</sup> The structures were solved by direct methods and subsequent difference Fourier syntheses, and refined using the SHELXTL software package.<sup>37</sup> The non-H atoms except for those which were found to be disordered were refined with anisotropic thermal parameters. Carbon-bound H atoms were placed in calculated positions and refined using a riding model. In the structure of **1**, the starting positions for methanol H atoms were located in difference Fourier syntheses, and then refined by using a geometrical model. In the case of **2**, the unit cell volume includes a large region of disordered solvent which could not be modeled as discrete atomic sites. PLATON/SQUEEZE<sup>20</sup> was employed to calculate the diffraction contribution of the solvent molecules and, thereby, to produce a set of solvent-free diffraction intensities. The final formulae were calculated from the SQUEEZE results combined with elemental analytical data.

**Crystal data for 1.** C<sub>35.50</sub>H<sub>31</sub>CoN<sub>3</sub>O<sub>9.50</sub>, *M* = 710.56, monoclinic, *a* = 12.565(2), *b* = 29.618(5), *c* = 9.858(2) Å, β = 105.695(3)°, *U* = 3531.9(11) Å<sup>3</sup>, *T* = 150(2) K, space group *P*2<sub>1</sub>/*c* (no. 14), *Z* = 4, 20276 reflections measured, 7379 unique (*R*<sub>int</sub> = 0.064) which were used in all calculations. Final *R*<sub>1</sub> = 0.114 [4137 *F* > 4σ(*F*)], *wR*<sub>2</sub> [all *F*<sup>2</sup>] = 0.298.

**Crystal data for 2.** C<sub>72</sub>H<sub>66</sub>Co<sub>2</sub>N<sub>10</sub>O<sub>18</sub>, *M* = 1477.21, triclinic, *a* = 10.090(2), *b* = 16.362(3), *c* = 24.453(5) Å, α = 106.75(3), β = 92.97(3), γ = 103.16(3)°, *U* = 3734(2) Å<sup>3</sup>, *T* = 150(2) K,

space group *P*1̄ (no. 2), *Z* = 4, 33315 reflections measured, 16720 unique (*R*<sub>int</sub> = 0.044) which were used in all calculations. Final *R*<sub>1</sub> = 0.0752 [8858 *F* > 4σ(*F*)], *wR*<sub>2</sub> [all *F*<sup>2</sup>] = 0.118. Selected bond lengths and angles are given in Table S2.†

### Powder X-ray diffraction

High resolution *in situ* synchrotron X-ray powder diffraction (PXRD) data were collected at Beamline I11 of Diamond Light Source using multi-analysing crystal-detectors (MACs) and monochromated radiation (λ = 0.82559 Å). These *in situ* diffraction measurements were carried out in capillary mode and the temperature controlled by an Oxford Cryosystems open-flow nitrogen gas cryostat. In a typical experiment, the powder sample of **1** was dried in air and ground for 10 min before loading into a capillary tube (0.7 mm diameter). Grinding provides a uniform and small (~20 micron) particle size essential for obtaining high-quality X-ray patterns. During the grinding process, some of the solvent content was lost from the pores. The capillary tube was connected to high vacuum (10<sup>-8</sup> mbar) and heated at 120 °C for ~2 h to generate the fully desolvated **1a** material. For each CO<sub>2</sub> pressure step, ~30–60 min were set for the equilibration time before collection of the PXRD pattern. The final PXRD pattern was collected after a final degassing for ~40 min to remove adsorbed CO<sub>2</sub> molecules. The poor crystallinity after desolvation and the complexity of the framework material meant that despite patterns being collected using synchrotron radiation at Diamond Light Source, the data quality was not sufficient to allow the use of Rietveld refinement to resolve the details of the structural changes.

### Isotherm simulation method

Grand Canonical Monte Carlo (GCMC) simulations were performed to calculate the adsorption of CO<sub>2</sub> in **1a**. Periodic boundary conditions were applied to a supercell (Fig. S14†), which contains six rigid (2×1×3) unit cells. The simulation parameters for CO<sub>2</sub> were taken from the TraPPE force field,<sup>38</sup> and the fugacity coefficients have been calculated from the Peng–Robinson equation of state.<sup>39</sup> The CO<sub>2</sub> molecule was assumed to have a C=O bond length of 1.16 Å and three charged Lennard–Jones interaction sites with the following parameters: σ<sub>O</sub> = 3.05 Å, ε<sub>O</sub>/k<sub>B</sub> = 79 K for oxygen atoms, and σ<sub>C</sub> = 2.80 Å and ε<sub>C</sub>/k<sub>B</sub> = 27 K for the carbon atom. A point charge of +0.7 was placed at the centre of mass of the carbon atom and a point charge of –0.35 was placed at the oxygen atoms. This model has been successfully used in the literature.<sup>40,41</sup> The parameters describing all the atoms were taken from the DREIDING forcefield<sup>42</sup> apart from Co, for which parameters from the Universal Force Field<sup>43</sup> were used. The charge distribution was calculated using the B3LYP level of theory and the 6-31G\* basis set. The structure used in the charge distribution calculations was a ligand with four different Co(II) centers as shown in Fig. 3 (top), with all dangling bonds saturated by methyl groups.

### Details of *in situ* IR apparatus

The *in situ* IR studies of **1a** were carried out in a high-pressure low temperature cell, which has been described in detail elsewhere.<sup>44</sup> A KBr disc with and without **1a** (ca. 5 mg) was used for

the matrix in the *in situ* IR experiments to record the spectra for the complex and background, respectively. **1a** was pressed into the surface of a preformed KBr disc. The discs were further degassed by heating to 60 °C under a high vacuum for 3 h and then mounted into the cell, which was then purged with Ar. The disc was placed under a vacuum, cooled to 195 K and then filled to various pressures between 0 and 1 bar of CO<sub>2</sub> (CP grade, supplied by BOC) to mimic the gas sorption experiments. For each pressure step, the equilibration time was set to ~30–60 min before the measurement of IR spectra. All IR spectra were recorded on a Nicolet Avatar 360 FTIR spectrometer with a liquid nitrogen cooled HgCdTe detector.

## Acknowledgements

SY gratefully acknowledges receipt of a Leverhulme Trust Early Career Research Fellowship, and MS acknowledges receipt of an ERC Advanced Grant and EPSRC Programme Grant. We thank the EPSRC and the University of Nottingham for funding. We are especially grateful to Diamond Light Source for access to Beamlines I11. MWG and NRC acknowledge receipt of Royal Society Wolfson Merit awards.

## Notes and references

- X. Lin, N. R. Champness and M. Schröder, *Top. Curr. Chem.*, 2010, **293**, 35–76.
- L. J. Murray, M. Dinca and J. R. Long, *Chem. Soc. Rev.*, 2009, **38**, 1294–1314.
- (a) B. L. Chen, C. D. Liang, J. Yang, D. S. Contreras, Y. L. Clancy, E. B. Lobkovsky, O. M. Yaghi and S. Dai, *Angew. Chem., Int. Ed.*, 2006, **45**, 1390–1393; (b) J. Li, R. J. Kuppler and H.-C. Zhou, *Chem. Soc. Rev.*, 2009, **38**, 1477–1504.
- J. S. Seo, D. Whang, H. Lee, S. I. Jun, J. Oh, Y. J. Jeon and K. Kim, *Nature*, 2000, **404**, 982–986.
- (a) P. Horcajada, C. Serre, G. Maurin, N. A. Ramsahye, F. Balas, M. Vallet-Regi, M. Sebban, F. Taulelle and G. Férey, *J. Am. Chem. Soc.*, 2008, **130**, 6774–6780; (b) J. Della Rocca, D. Liu and W. Lin, *Acc. Chem. Res.*, 2011, **44**, 957–968; (c) R. C. Huxford, K. E. deKrafft, W. S. Boyle, D. Liu and W. Lin, *Chem. Sci.*, 2012, **3**, 198–204; (d) K. M. L. Taylor-Pashow, J. Della Rocca, Z. Xie, S. Tran and W. Lin, *J. Am. Chem. Soc.*, 2009, **131**, 14261–14263.
- (a) X. Lin, I. Telepeni, A. J. Blake, A. Dailly, C. M. Brown, J. M. Simmons, M. Zoppi, G. S. Walker, K. M. Thomas, T. J. Mays, P. Hubberstey, N. R. Champness and M. Schröder, *J. Am. Chem. Soc.*, 2009, **131**, 2159–2171; (b) S. Yang, X. Lin, A. Dailly, A. J. Blake, N. R. Champness, P. Hubberstey and M. Schröder, *Chem.–Eur. J.*, 2009, **15**, 4829–4835.
- B. L. Chen, N. W. Ockwig, A. R. Millward, D. S. Contreras and O. M. Yaghi, *Angew. Chem., Int. Ed.*, 2005, **44**, 4745–4749.
- S. Horike, S. Shimomura and S. Kitagawa, *Nat. Chem.*, 2009, **1**, 695–704.
- S. Kitagawa and K. Uemura, *Chem. Soc. Rev.*, 2005, **34**, 109–119.
- B. Kesanli and W. Lin, *Coord. Chem. Rev.*, 2003, **246**, 305–326.
- Y. Goto, H. Sato, S. Shinkai and K. Sada, *J. Am. Chem. Soc.*, 2008, **130**, 14354–14355.
- K. L. Mulfort, O. K. Farha, C. L. Stern, A. A. Sarjeant and J. T. Hupp, *J. Am. Chem. Soc.*, 2009, **131**, 3866–3868.
- Z. Q. Wang and S. M. Cohen, *J. Am. Chem. Soc.*, 2007, **129**, 12368–12369.
- A. D. Burrows, C. G. Frost, M. F. Mahon and C. Richardson, *Angew. Chem., Int. Ed.*, 2008, **47**, 8482–8486.
- H. X. Deng, C. J. Doonan, H. Furukawa, R. B. Ferreira, J. Towne, C. B. Knobler, B. Wang and O. M. Yaghi, *Science*, 2010, **327**, 846–850.
- L. Ma and W. Lin, *Top. Curr. Chem.*, 2010, **293**, 175–205.
- L. J. Goossen, G. Deng and L. M. Levy, *Science*, 2006, **313**, 662–664.
- J. Li and T. B. Brill, *J. Phys. Chem. A*, 2002, **106**, 9491–9498.
- C. Bonneau, O. Delgado-Friedrichs, M. O’Keeffe and O. M. Yaghi, *Acta Crystallogr., Sect. A: Found. Crystallogr.*, 2004, **60**, 517–520.
- A. L. Spek, *Acta Crystallogr., Sect. D: Biol. Crystallogr.*, 2009, **65**, 148–155.
- O. K. Farha, A. O. Yazaydin, I. Eryazici, C. D. Malliakas, B. G. Hauser, M. G. Kanatzidis, S. T. Nguyen, R. Q. Snurr and J. T. Hupp, *Nat. Chem.*, 2010, **2**, 944–948.
- H. Furukawa, N. Ko, Y. B. Go, N. Aratani, S. B. Choi, E. Choi, A. O. Yazaydin, R. Q. Snurr, M. O’Keeffe, J. Kim and O. M. Yaghi, *Science*, 2010, **329**, 424–428.
- (a) Y. Yan, X. Lin, S. Yang, A. J. Blake, A. Dailly, N. R. Champness, P. Hubberstey and M. Schröder, *Chem. Commun.*, 2009, 1025–1027; (b) Y. Yan, I. Telepeni, S. Yang, X. Lin, W. Kockelmann, A. Dailly, A. J. Blake, W. Lewis, G. S. Walker, D. R. Allan, S. A. Barnett, N. R. Champness and M. Schröder, *J. Am. Chem. Soc.*, 2010, **132**, 4092–4094; (c) Y. Yan, S. Yang, A. J. Blake, W. Lewis, E. Poirier, S. A. Barnett, N. R. Champness and M. Schröder, *Chem. Commun.*, 2011, **47**, 9995–9997; (d) C. Tan, S. Yang, X. Lin, A. J. Blake, W. Lewis, N. R. Champness and M. Schröder, *Chem. Commun.*, 2011, **47**, 4487–4489; (e) Y. Yan, A. J. Blake, W. Lewis, S. A. Barnett, A. Dailly, N. R. Champness and M. Schröder, *Chem.–Eur. J.*, 2011, **17**, 11162–11170; (f) S. Yang, X. Lin, W. Lewis, M. Suyetin, E. Bichoutskaia, J. E. Parker, C. C. Tang, D. R. Allan, P. J. Rizkallah, P. Hubberstey, N. R. Champness, K. M. Thomas, A. J. Blake and M. Schröder, *Nat. Mater.*, 2012, DOI: 10.1038/NMAT3343.
- C. Serre, F. Millange, C. Thouvenot, M. Nogues, G. Marsolier, D. Louer and G. Férey, *J. Am. Chem. Soc.*, 2002, **124**, 13519–13526.
- S. Bourrelly, P. L. Llewellyn, C. Serre, F. Millange, T. Loiseau and G. Férey, *J. Am. Chem. Soc.*, 2005, **127**, 13519–13521.
- G. J. Halder and C. J. Kepert, *J. Am. Chem. Soc.*, 2005, **127**, 7891–7900.
- F. X. Coudert, M. Jeffroy, A. H. Fuchs, A. Boutin and C. Mellot-Draznieks, *J. Am. Chem. Soc.*, 2008, **130**, 14294–14302.
- C. Serre, S. Bourrelly, A. Vimont, N. A. Ramsahye, G. Maurin, P. L. Llewellyn, M. Daturi, Y. Filinchuk, O. Leynaud, P. Barnes and G. Férey, *Adv. Mater.*, 2007, **19**, 2246–2251.
- Z. Wang and S. M. Cohen, *J. Am. Chem. Soc.*, 2009, **131**, 16675–16677.
- S. Lim, H. Kim, N. Selvapalam, K. J. Kim, S. J. Cho, G. Seo and K. Kim, *Angew. Chem., Int. Ed.*, 2008, **47**, 3352–3355.
- R. Matsuda, R. Kitaura, S. Kitagawa, Y. Kubota, R. V. Belosludov, T. C. Kobayashi, H. Sakamoto, T. Chiba, M. Takata, Y. Kawazoe and Y. Mita, *Nature*, 2005, **436**, 238–241.
- C. R. Reid and K. M. Thomas, *Langmuir*, 1999, **15**, 3206–3218.
- J. Zhang and S. Kitagawa, *J. Am. Chem. Soc.*, 2008, **130**, 907–917.
- D. Tanaka, M. Higuchi, S. Horike, R. Matsuda, Y. Kinoshita, N. Yanai and S. Kitagawa, *Chem.–Asian J.*, 2008, **3**, 1343–1349.
- M. Fischer, F. Hoffmann and M. Fréchet, *ChemPhysChem*, 2010, **11**, 2220–2229.
- G. M. Sheldrick, *SADABS, Program for area detector adsorption correction*, Institute for Inorganic Chemistry, University of Göttingen, Germany, 1996.
- G. M. Sheldrick, *Acta Crystallogr., Sect. A: Found. Crystallogr.*, 2008, **64**, 112–122.
- J. J. Potoff and J. I. Siepmann, *AIChE J.*, 2002, **47**, 1676–1682.
- D. Y. Peng and D. B. Robinson, *Ind. Eng. Chem. Fundam.*, 1976, **15**, 59–64.
- Q. Yang and C. Zhong, *ChemPhysChem*, 2006, **7**, 1417–1421.
- J. R. Karra and K. S. Walton, *J. Phys. Chem. C*, 2010, **114**, 15735–15740.
- S. L. Mayo, B. D. Olafson and W. A. Goddard III, *J. Phys. Chem.*, 1990, **94**, 8897–8909.
- A. B. Rappe, C. J. Casewit, K. S. Colwell, W. A. Goddard III and W. M. Skid, *J. Am. Chem. Soc.*, 1992, **114**, 10024–10035.
- A. I. Cooper and M. Poliakoff, *Chem. Phys. Lett.*, 1993, **212**, 611–616.